

## Thermal expansion and phonon anharmonicity of cuprite studied by inelastic neutron scattering and *ab initio* calculations

C. N. Saunders<sup>1,\*</sup>, D. S. Kim<sup>2</sup>, O. Hellman<sup>3,4</sup>, H. L. Smith<sup>5</sup>, N. J. Weadock<sup>6</sup>, S. T. Omelchenko<sup>1</sup>, G. E. Granroth<sup>7</sup>,  
C. M. Bernal-Choban<sup>1</sup>, S. H. Lohaus<sup>1</sup>, D. L. Abernathy<sup>7</sup> and B. Fultz<sup>1,†</sup>

<sup>1</sup>*Department of Applied Physics and Materials Science, California Institute of Technology, Pasadena, California 91125, USA*

<sup>2</sup>*Department of Materials Science and Engineering, Massachusetts Institute of Technology, Cambridge, Massachusetts 02139, USA*

<sup>3</sup>*Department of Physics, Chemistry, and Biology (IFM), Linköping University, SE-581 83 Linköping, Sweden*

<sup>4</sup>*Department of Molecular Chemistry and Material Science, Weizmann Institute of Science, Rehovot 76100, Israel*

<sup>5</sup>*Department of Physics and Astronomy, Swarthmore College, Swarthmore, Pennsylvania 19081, USA*

<sup>6</sup>*Department of Chemical and Biological Engineering, University of Colorado Boulder, Boulder, Colorado 80309, USA*

<sup>7</sup>*Neutron Scattering Division, Oak Ridge National Laboratory (ORNL), Oak Ridge, Tennessee 37831, USA*

 (Received 22 June 2021; revised 24 November 2021; accepted 10 May 2022; published 31 May 2022)

Inelastic neutron scattering measurements were performed with a time-of-flight chopper spectrometer to observe phonons in all parts of the Brillouin zone of a single crystal of cuprite  $\text{Cu}_2\text{O}$ . We reduced the experimental data to phonon dispersions in the high-symmetry directions, and changes between 10 and 300 K are reported. In this paper, we show *ab initio* quasiharmonic (QH) and anharmonic (AH) calculations of phonon dispersions. We performed all AH calculations with a temperature-dependent effective potential method. Both QH and AH calculations account for the small negative thermal expansion of cuprite at low temperatures. However, the measured temperature-dependent phonon behavior was predicted more accurately with the AH calculations than the QH ones. Nevertheless, at 300 K, the cubic AH used in this paper did not entirely account for the experimental phonon dispersions in cuprite.

DOI: [10.1103/PhysRevB.105.174308](https://doi.org/10.1103/PhysRevB.105.174308)

### I. INTRODUCTION

Cuprite  $\text{Cu}_2\text{O}$  (Fig. 1) is one of the first known semiconductors [1,2]. It has applications in photovoltaics [3,4], nanoelectronics [5], thermoelectrics [6], spintronics [7], and catalysis [8,9]. Cuprite has a small coefficient of thermal expansion that is negative at low temperatures but becomes positive  $>300$  K. The coefficient of volumetric thermal expansion  $\beta = \frac{1}{V} \frac{\partial V}{\partial T}$  ( $V$  is volume, and  $T$  is temperature) is explained with thermodynamics by a balance between the internal energy  $U$  and the entropy  $S$ . At finite temperatures, the primary contributions to  $U$  and  $S$  are the elastic energy ( $U_{\text{el}}$ ) and the vibrational entropy of phonons ( $S_{\text{vib}}$ ). Using this approximation, the total free energy  $F = U_{\text{el}} - TS_{\text{vib}}$  is minimized when reductions in the phonon frequencies with volume (and temperature) cause a larger  $S_{\text{vib}}$ . These changes counteract the energy penalty from  $U_{\text{el}}$  during thermal expansion.

Spectroscopies to study phonons include inelastic neutron, inelastic x-ray, and Raman methods. All of these methods have been used to study phonons in cuprite [11–30]. Inelastic neutron scattering (INS) experiments with triple-axis spectrometers measure energy spectra of phonons at single points in crystal momentum  $\vec{q}$ . Thermophysical properties such as thermal expansion and the temperature dependence of elastic constants depend on the phonon frequencies at all  $\vec{q}$  points in the first Brillouin zone. Methods of INS on single

crystals at pulsed neutron sources can provide such detailed information [31,32]. Measurements of all phonons in a crystal allow testing of microscopic models of thermophysical properties.

The free energy  $F_{\text{vib}}$  in the anharmonic (AH) theory used here is

$$F_{\text{vib}}(V, T) = U_0(V, T) + \sum_{\vec{q},s} \left( \frac{\hbar\omega_{\vec{q},s}(V, T)}{2} + k_{\text{B}}T \ln \left\{ 1 - \exp \left[ -\frac{\hbar\omega_{\vec{q},s}(V, T)}{k_{\text{B}}T} \right] \right\} \right), \quad (1)$$

where the phonon frequencies  $\omega_{\vec{q},s}$  ( $s$  is a branch index) depend on both  $V$  and  $T$ . An explicit dependence on  $T$  is essential for AH models. The quasiharmonic (QH) vibrational Helmholtz free energy contribution  $F_{\text{vib}}$  depends explicitly on  $V$ , and effects of  $T$  are only through thermal expansion  $\omega_{\vec{q},s}[V(T)]$  rather than  $\omega_{\vec{q},s}(V, T)$  for AH theory. Phonons in materials can be modeled or interpreted with QH or AH theories [33].

In this paper, we identify the microscopic physics of the individual phonon modes that contribute to the macroscopic thermal expansion. We do this by calculating individual phonon contributions to  $F_{\text{vib}}$  with both QH and AH theories and comparing the thermal trends of the calculated phonons with phonon measurements by INS on cuprite at 10 and 300 K. The net volume change of cuprite from thermal expansion between 10 and 300 K is small, so QH calculations predict phonon shifts that are nearly zero. On the other hand, experiment and AH calculations give thermal shifts and

\*clairenicolesaunders@gmail.com

†btf@caltech.edu

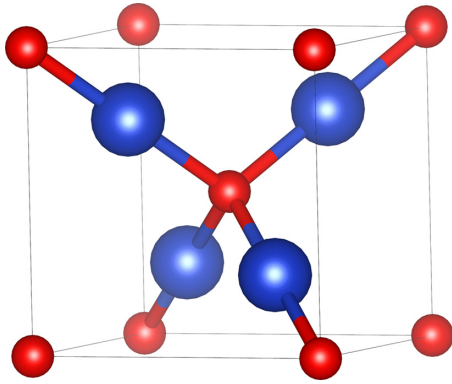


FIG. 1. Unit cell of  $\text{Cu}_2\text{O}$ . Copper (Cu) atoms are shown in blue and oxygen (O) atoms in red. There is a linear arrangement of O-Cu-O as the  $3z^2-r^2$  orbitals of copper make chemical bonds with the  $sp^3$  orbitals of oxygen [10].

broadening phonons, especially optical modes. However, we expect the low-frequency acoustic modes to be more pertinent to the negative thermal expansion (NTE) at low temperatures. We found small but measurable changes in the acoustic phonons between 10 and 300 K. Closer examination shows that QH theory predicts changes in both magnitude and sign of the thermal shifts of the lowest acoustic branch at different  $\vec{q}$ . On the other hand, AH theory and experiment show that this entire branch undergoes a thermal shift that is nearly the same at all  $\vec{q}$ .

## II. EXPERIMENT

### A. Powder

INS measurements were performed first on 20 g  $\text{Cu}_2\text{O}$  powder with the time-of-flight (TOF) wide angular-range chopper spectrometer (ARCS) [31] at the Spallation Neutron Source at Oak Ridge National Laboratory (ORNL) [34]. The incident energy was 120 meV, and sample temperatures were 5 and 300 K. Using the software packages MANTID and MULTIPHONON, we reduced the data to phonon density of states (DOS) curves [35,36]. The reduction included subtractions of an empty aluminum can background and a multiphonon correction.

### B. Single crystal

Further INS measurements used ARCS to perform measurements on a single crystal of cuprite. The [100]-oriented single crystal was grown at the Joint Center for Artificial Photosynthesis at Caltech in an optical furnace with the float zone method [37] with 99.999% Cu rods from Alfa Aesar. The crystal was a cylinder of 50 mm in height and 7 mm in diameter, suspended in a platinum holder for all measurements. See the Supplemental Material [38] for images of the crystal and mount (see also Refs. [29,39–44] therein).

For 10 K measurements, the crystal was in an aluminum canister within a closed-cycle helium refrigerator. TOF neu-

tron spectra were acquired at 152 individual angles of the crystal in increments of  $0.5^\circ$ , about the vertical axis. For 300 K measurements, we mounted the crystal in a low-background electrical resistance vacuum furnace [45]. Measurements at 300 K used 201 angles in increments of  $0.5^\circ$ . The incident energy for all single-crystal measurements was 110 meV. An oscillating radial collimator suppressed multiple scattering and background.

To reduce the single-crystal data to obtain the four-dimensional  $S(\vec{Q}, \varepsilon)$ , we used MANTID. An additional analysis assessed the data statistics and alignment. Following crystal symmetry, we folded the data from high  $\vec{Q}$  into the irreducible wedge in the first Brillouin zone. An averaged multiphonon scattering correction was subtracted from the data, and spectral weights were thermal factor corrected. The results of our analysis appear in Fig. 2 with further details of data postprocessing available in the Supplemental Material [38] (see, also Refs. [29,39–44] therein).

## III. COMPUTATION

The Vienna *Ab initio* Simulation Package (VASP) was used for all *ab initio* density functional theory calculations [46–49] with plane-wave basis sets, projector augmented wave pseudopotentials [50] and the strongly constrained and appropriately normed meta-generalized gradient approximation exchange correlation functional [51]. All calculations used  $3 \times 3 \times 3$  supercells containing 162 atoms, a  $2 \times 2 \times 2$   $k$ -grid, and a kinetic energy cutoff of 600 eV. The supercell configurations for calculations were generated with the stochastic temperature-dependent effective potential (sTDEP) method or PHONOPY [52]. For further details on calculation parameters, see the Supplemental Material [38].

We found the equilibrium volume for each temperature by minimizing the Helmholtz free energy, which included electronic and phononic contributions, for five volumes ( $\pm 1.5\%$ ,  $\pm 3.0\%$ , and the 0 K equilibrium volume). For each volume, we performed QH calculations with PHONOPY. All QH calculations used the finite displacement method. AH calculations used the sTDEP package [53–55]. Finally, we fit the Helmholtz free energy to the Birch-Murnaghan equation of state. The minimum of this function provided the equilibrium volume at the temperature of interest.

AH effects on the lattice parameter and on phonons are accounted for in  $U_0(T, V)$  and  $\omega_{\vec{q},s}(T, V)$ . The expression for  $U_0(T, V)$  in our AH thermal expansion calculations is

$$U_0(V, T) = \left\langle U_{\text{BO}}(V, T) - \frac{1}{2} \sum_{ij} \sum_{\alpha\beta} \Phi_{ij}^{\alpha\beta} u_i^\alpha u_j^\beta \right\rangle, \quad (2)$$

where  $U_{\text{BO}}(T, V)$  is the Born-Oppenheimer potential energy from sampling the surface, and  $\Phi_{ij}^{\alpha\beta}$  are forces that are matched between the actual system and with our model Hamiltonian. Here,  $u_i^\alpha$  and  $u_j^\beta$  are Cartesian components of the displacements of atoms  $i$  and  $j$ . When accounting for third-order terms for phonon self-energies,

$$U_0(V, T) = \left\langle U_{\text{BO}}(V, T) - \frac{1}{2!} \sum_{ij} \sum_{\alpha\beta} \Phi_{ij}^{\alpha\beta} u_i^\alpha u_j^\beta - \frac{1}{3!} \sum_{ijk} \sum_{\alpha\beta\gamma} \Phi_{ijk}^{\alpha\beta\gamma} u_i^\alpha u_j^\beta u_k^\gamma \right\rangle. \quad (3)$$

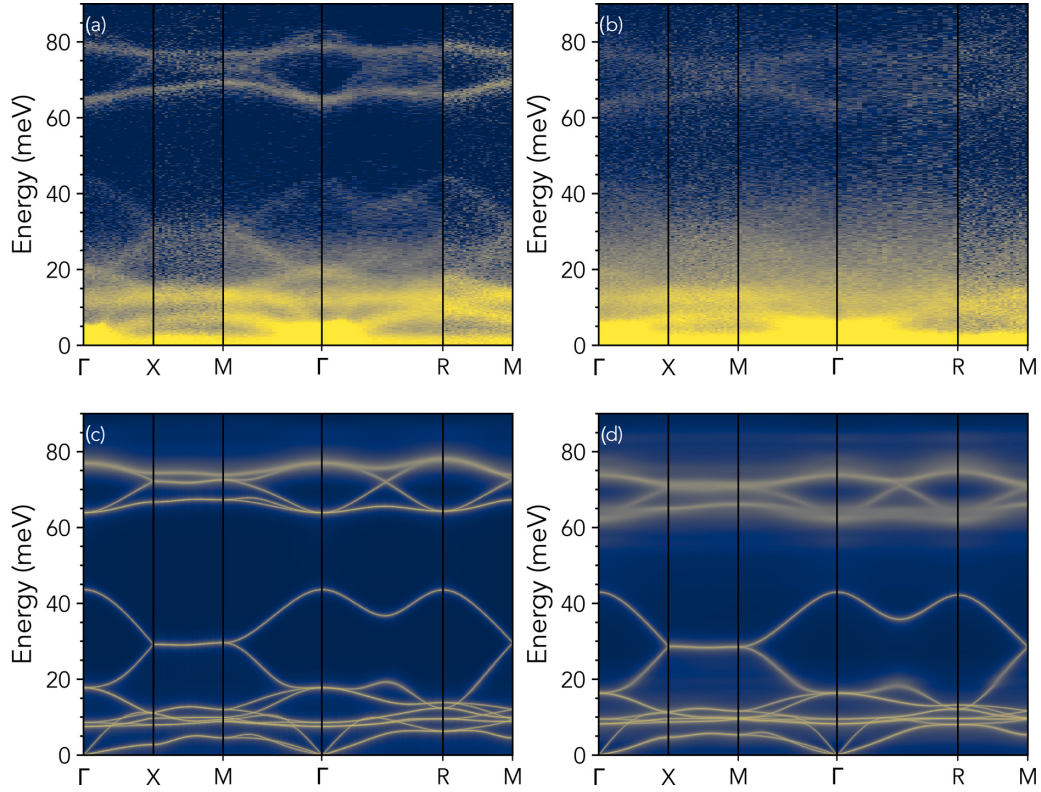


FIG. 2. Phonon dispersions along high-symmetry directions measured by inelastic neutron scattering (INS) at (a) 10 K and (b) 300 K. Phonon dispersions calculated by sTDEP at (c) 10 K and (d) 300 K.

After obtaining the lattice parameter, we calculated the phonon dispersions and self-energy at that volume.

Authors of previous studies of lattice dynamics and the NTE of cuprite used the QH approximation. In QH theory, each phonon mode  $s$  with corresponding angular frequency  $\omega_{\vec{q},s}$  depends directly on the volume through the mode Grüneisen parameter  $\gamma_{\vec{q},s}$  at a given wave vector  $\vec{q}$ :

$$\gamma_{\vec{q},s}(V) = -\frac{V}{\omega_{\vec{q},s}(V)} \frac{\partial \omega_{\vec{q},s}(V)}{\partial V}. \quad (4)$$

Equation (4) predicts thermal shifts of individual phonon frequencies. An average  $\gamma$ , where each  $\gamma_{\vec{q},s}$  is weighted by the contribution of phonon  $s$  to the heat capacity, predicts the macroscopic thermal expansion. Average phonon frequencies decrease for positive values of  $\gamma$  as volume increases. This decrease in  $\omega_{\vec{q},s}$  contributes positively to the vibrational entropy  $S_{\text{vib}}$  and lowers the QH vibrational Helmholtz free energy  $F^{\text{QH}}$ .

For AH computations, where third-order force constants are available [56], the mode Grüneisen parameters for a mode

with frequency  $\omega_{\vec{q},s}$  is

$$\gamma_{\vec{q},s}(V, T) = -\frac{V}{6\omega_{\vec{q},s}(V, T)^2} \times \sum_{ijk\alpha\beta\gamma} \frac{\epsilon_{\vec{q},s}^{i\alpha\dagger} \epsilon_{\vec{q},s}^{j\beta}}{\sqrt{m_i m_j}} r_k^\gamma \Phi_{ijk}^{\alpha\beta\gamma} \exp(\vec{q} \cdot \vec{r}_j). \quad (5)$$

Here,  $\Phi_{ijk}^{\alpha\beta\gamma}$  is the cubic AH tensor with Cartesian indices  $\alpha$ ,  $\beta$ , and  $\gamma$ . Also,  $\epsilon$  is the polarization eigenvector, and atomic position and mass are designed by  $\vec{r}$  and  $m$ , respectively. Equation (5) offers an advantage over Eq. (4) because it is not divergent when the thermal expansion is zero, so the mode Grüneisen parameters were calculated using Eq. (5). All calculations were performed in sTDEP using the third-order force constants.

The calculated phonon self-energy gives phonon spectra with thermal shifts and finite linewidths. Calculations of this include terms to the third power of atom displacements (cubic AH) [57,58]. We performed AH calculations of the self-energy with sTDEP. By solving a dynamical matrix, we obtained phonon frequencies. For a given third-order force constant  $\Phi_{ss's''}$ , we calculated and adjusted the phonon self-energy with the real  $\Delta$  and imaginary  $\Gamma$  corrections

to the phonon self-energy. The imaginary correction is

$$\Gamma_{ss's''}^{\vec{q}\vec{q}'}(V, T) = \frac{\hbar\pi}{16} \sum_{ss's''} |\Phi_{ss's''}^{\vec{q}\vec{q}'}|^2 (n_{\vec{q}',s'} + n_{\vec{q},s''} + 1) \delta(\Omega - \omega_{\vec{q}',s'} - \omega_{\vec{q},s''}) + (n_{\vec{q},s'} - n_{\vec{q}',s''}) [\delta(\Omega - \omega_{\vec{q},s'} + \omega_{\vec{q}',s''}) - \delta(\Omega + \omega_{\vec{q},s'} - \omega_{\vec{q}',s''})], \quad (6)$$

where  $\hbar\Omega$  is a probing energy,  $\omega_{\vec{q},s}^2$  are the eigenvalues of the dynamical matrix, and  $n$  are the occupancy factors. The three-phonon matrix component can be written as

$$\Phi_{ss's''}^{\vec{q}\vec{q}'\vec{q}''} = \sum_{ijk} \sum_{\alpha\beta\gamma} \frac{\epsilon_s^{i\alpha} \epsilon_{s'}^{j\beta} \epsilon_{s''}^{k\gamma}}{\sqrt{m_i m_j m_k} \sqrt{\omega_{\vec{q},s} \omega_{\vec{q}',s'} \omega_{\vec{q}'',s''}}} \Phi_{ijk}^{\alpha\beta\gamma} \exp[i(\vec{q} \cdot \vec{r}_i + \vec{q}' \cdot \vec{r}_j + \vec{q}'' \cdot \vec{r}_k)], \quad (7)$$

where the primes help identify the three-phonon interactions. Remaining indices are defined after Eq. (5).

The real part of the phonon self-energy correction is obtained from the Kramers-Kronig transform:

$$\Delta_{\vec{q},s}(\Omega_{\vec{q},s}) = \frac{1}{\pi} \int \frac{\Gamma(\omega_{\vec{q},s})}{\omega_{\vec{q},s} - \Omega} d\omega_{\vec{q},s}. \quad (8)$$

Large deviations of  $\Delta_{\vec{q},s}(\Omega_{\vec{q},s})$  from Lorentzian functions suggest a high degree of AH.

In the QH approximation, Eq. (1) reduces to

$$F_{\text{vib}}^{\text{QH}}(V, T) = U_0(V) + \sum_{\vec{q},s} \left( \frac{\hbar\omega_{\vec{q},s}(V)}{2} + k_B T \ln \left[ 1 - \exp \left[ -\frac{\hbar\omega_{\vec{q},s}(V)}{k_B T} \right] \right] \right). \quad (9)$$

In the QH approximation, phonon frequencies and ground state energy do not have explicit temperature dependence, but  $V = V(T)$  with thermal expansion.

#### IV. RESULTS

Figure 2 shows phonon spectra from INS measurements and AH calculations along the high-symmetry crystallographic directions. Figures 2(a) and 2(b) show the folded experimental data from the single crystal at 10 and 300 K, respectively, and Figs. 2(c) and 2(d) show the corresponding AH sTDEP calculations. The main features and energies of the calculated and measured intensities agree. Both calculated and measured data show softening of the high-energy optical modes. However, the calculated softening of these modes is larger than the experimental results. Below 45 meV, small changes in the calculated and measured dispersions follow the same thermal trends.

Figure 3(b) shows the phonon partial DOS curves for Cu and O atoms in cuprite, calculated by sTDEP. The O atoms dominate the spectral weight in the high-energy modes between 65 and 80 meV, and Cu atoms dominate  $<45$  meV. Their sum agrees with the experimental spectra from INS measurements shown in Fig. 3(a), without neutron-weight corrections. Figure 4 compares experimental cuts taken at single  $\vec{q}$  points along high-symmetry paths with cuts calculated with sTDEP and with energies from PHONOPY. The AH sTDEP results show thermal shifts, but the QH PHONOPY calculations display no discernible changes with the temperature on the scale of Fig. 4. Grüneisen parameters from sTDEP with Eq. (5) are shown in Figs. 5(a) and 5(c) at different temperatures. These Grüneisen parameters are in good agreement with prior QH calculations and experimental results [59]. The plots are color-coded, so the Grüneisen parameters for each mode correspond to the same color mode in the dispersions in Figs. 5(b) and 5(d). Many of the low-energy dispersions have negative Grüneisen parameters, including the low-energy transverse acoustic (TA) modes that are useful for explaining the NTE in QH theory. The high-energy optical modes have positive Grüneisen parameters, but these are like the Grüneisen parameters of other phonon branches. Modes with

similar Grüneisen parameters are predicted by QH theory to have similar thermal shifts. The real and imaginary parts of the phonon self-energy at the point  $\vec{Q} = (0.25, 0.25, 0.00)$  appear in Fig. 6, colored in correspondence with their phonon branches in Fig. 5. Significant deviations from the harmonic self-energy for the optical modes with energies  $>70$  meV show that these modes are more AH than the other modes. There are also substantial AH effects from cubic AH for the lower-energy optical modes  $\sim 40$  meV. Comparing the partial DOS with the self-energies shows that the displacements of oxygen atoms dominate these AH modes.

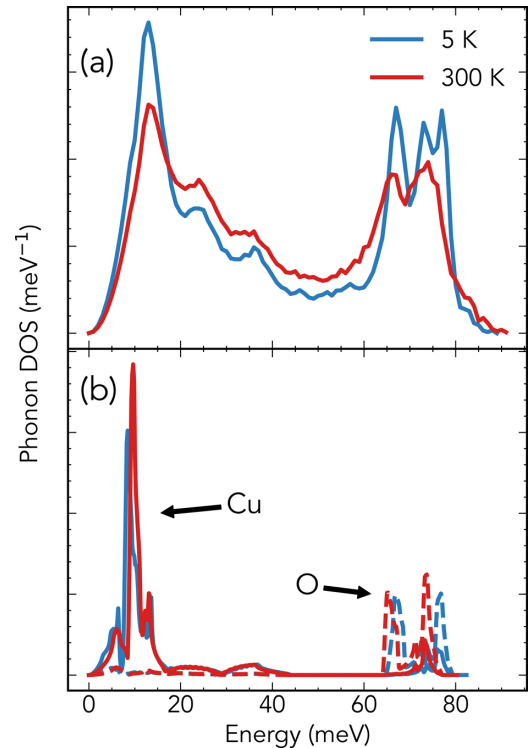


FIG. 3. (a) Phonon density of states (DOS) from inelastic neutron scattering (INS) measurements on powdered cuprite. (b) Phonon partial DOS from sTDEP calculations using second-order terms at 10 and 300 K. Solid curves are Cu atoms, dashed are O atoms.

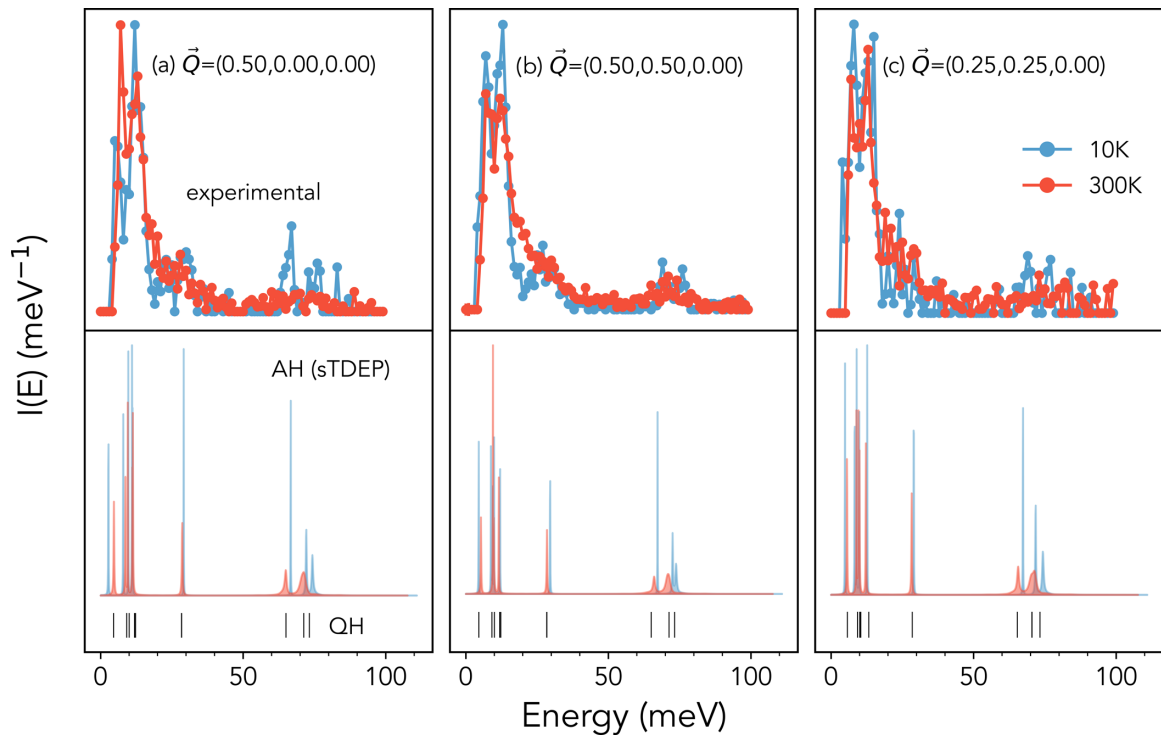


FIG. 4. Energy spectra at three values of  $\vec{Q}$  at 10 K (blue) and 300 K (red). (a) Energy cut at the  $X$  point for experimental (top panel), anharmonic (AH) calculations (lower panel), and quasiharmonic (QH) calculations (lower panel, black lines) at labeled temperatures. (b) Energy cut at the  $M$  point. (c) Energy cut at the halfway point between the high-symmetry points  $X$  and  $M$ . The color specifies the experimental and AH data temperatures. Both temperatures of the QH data are denoted by black at the bottom because there is no discernible change of QH phonons between 10 and 300 K.

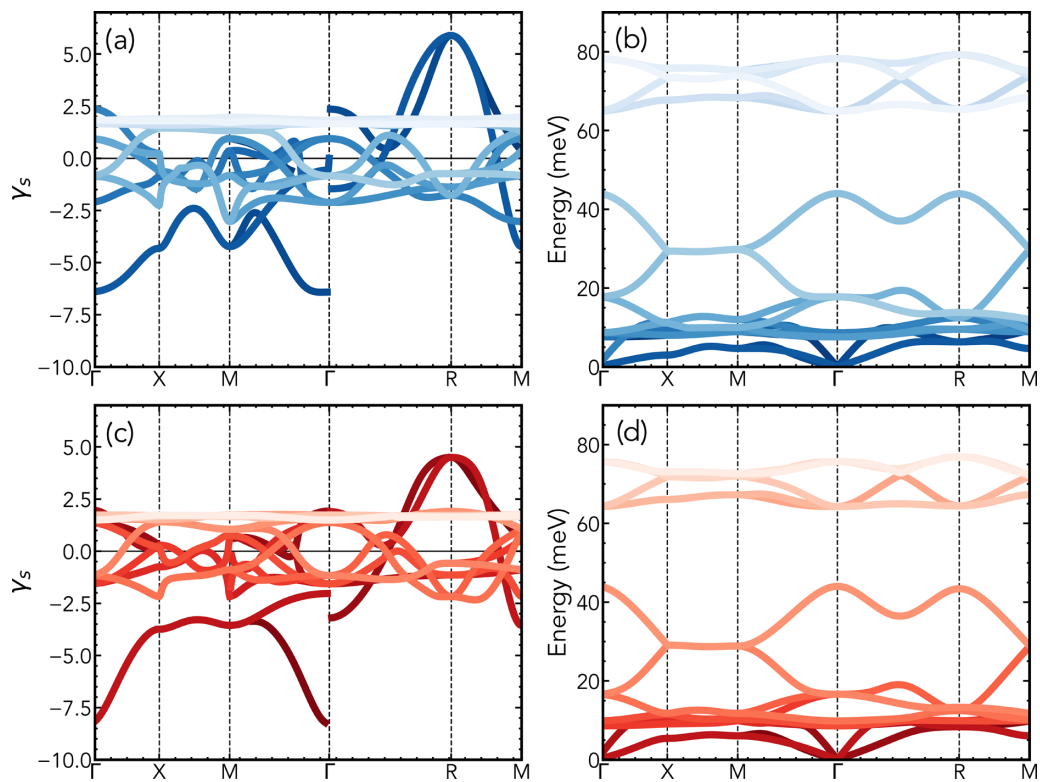


FIG. 5. Mode Grüneisen parameters for dispersions, shaded to match their corresponding dispersions at (a) 10 K and (c) 300 K. Phonon dispersions from quadratic terms in sTDEP calculations at (b) 10 K and (d) 300 K colored to correspond with their matching mode Grüneisen parameters.

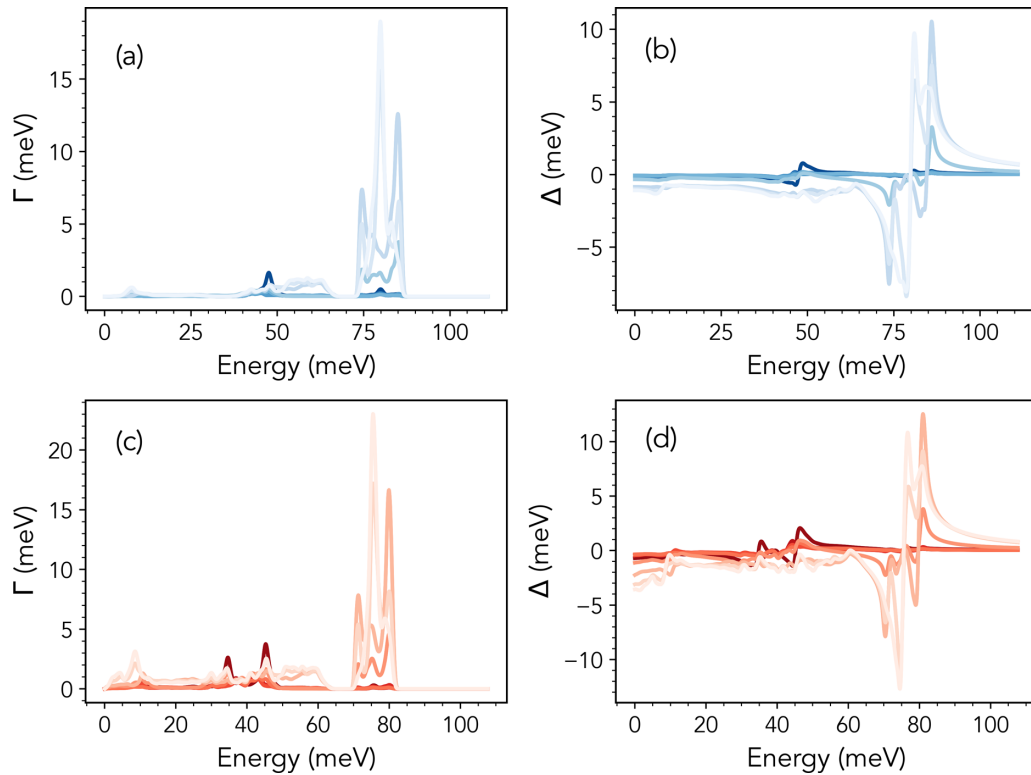


FIG. 6. The imaginary part ( $\Gamma$ ) of the phonon self-energy at (a) 10 K in blue and (c) 300 K shown in red. Different shades of red and blue correspond to individual modes designated by Figs. 5(b) and 5(d) for the real part ( $\Delta$ ) of the phonon self-energy. Data are for  $\vec{Q} = (0.25, 0.25, 0.0)$ .

Figure 7 shows the percentage change in lattice parameter of cuprite vs temperature, referenced to a nominal 0 K. Panel (a) compares the sTDEP lattice parameter with experimental results, and panel (b) compares it with our QH calculations and other QH calculations in the literature. Both QH and AH calculations  $< 250$  K reproduce the measured NTE. However, the thermal expansion coefficient in this region is small, no larger than  $-2.4 \times 10^{-6}/\text{K}$ , and is zero near 250 K.

## V. DISCUSSION

The AH sTDEP calculations better predict the measured effect of temperature on cuprite phonons than QH PHONOPY calculations, as seen in the energy cuts of Fig. 4. For cuprite, Grüneisen parameters from sTDEP and QH calculations are essentially the same [59]. In the QH approximation, phonon shifts follow the  $\vec{q}$  dependence of the Grüneisen parameters shown in Fig. 5, which is not the thermal trend of the phonon branches. There are two key differences. First, the phonon frequencies depend solely on volume in QH theory, so it predicts a negligible difference between calculated dispersions at 10 and 300 K. While the thermal shifts are small, they are measurable and larger than predicted by QH calculations. A second problem appears in Fig. 5. For the low TA branch at the  $X$  point, the Grüneisen parameter is  $-4$ , whereas it is  $\sim +5$  at the  $R$  point. However, the entire low-TA branch in the experimental results (and sTDEP) in Fig. 2 shifts upward in energy with temperature between 10 and 300 K, as shown

in Fig. 4. There are no observable differences in the behavior at the  $X$  or  $R$  points. The Grüneisen parameters for the low-energy optical branches also change signs at different  $\vec{q}$ , but the branches from sTDEP have simple behavior. The modes  $< 11$  meV shift up with temperature, and those  $> 11$  meV shift down with temperature.

Authors of previous studies of cuprite showed the success of QH theory for predicting thermal expansion [59,61–64], and some studies included results on phonon dynamics [61,62,65]. We find similar success with QH theory for thermal expansion and with AH theory. These results seem like those of a previous study on the thermal expansion of silicon, another small NTE material, which showed that AH effects dominate over QH effects for thermal phonon shifts at low temperatures [32,66].

The thermal expansion from Eq. (1) depends only on the temperature dependence of  $U$  through the electronic energy and the temperature dependence of  $S$  through the phonon frequencies  $d\omega_{\vec{q},s}/dT$ . With AH,  $\omega_{\vec{q},s}$  depends independently on both  $T$  and  $V$ . In QH, we assume  $\omega_{\vec{q},s}[V(T)]$ , so all effects from  $T$  originate solely with  $\Delta V = \beta TV$ . The QH approximation gives generally good results for thermal expansion, as shown in Fig. 7, even though it does not reliably predict the  $d\omega_{\vec{q},s}/dT$  (for many phonons, the  $d\omega_{\vec{q},s}/dT$  in the QH approximation has the wrong sign). With its prediction of tiny shifts in phonon frequencies between 10 and 300 K, it is difficult to pinpoint why the QH approximation might successfully predict the thermal expansion. Perhaps its success originates from a fortuitous cancellation of errors.

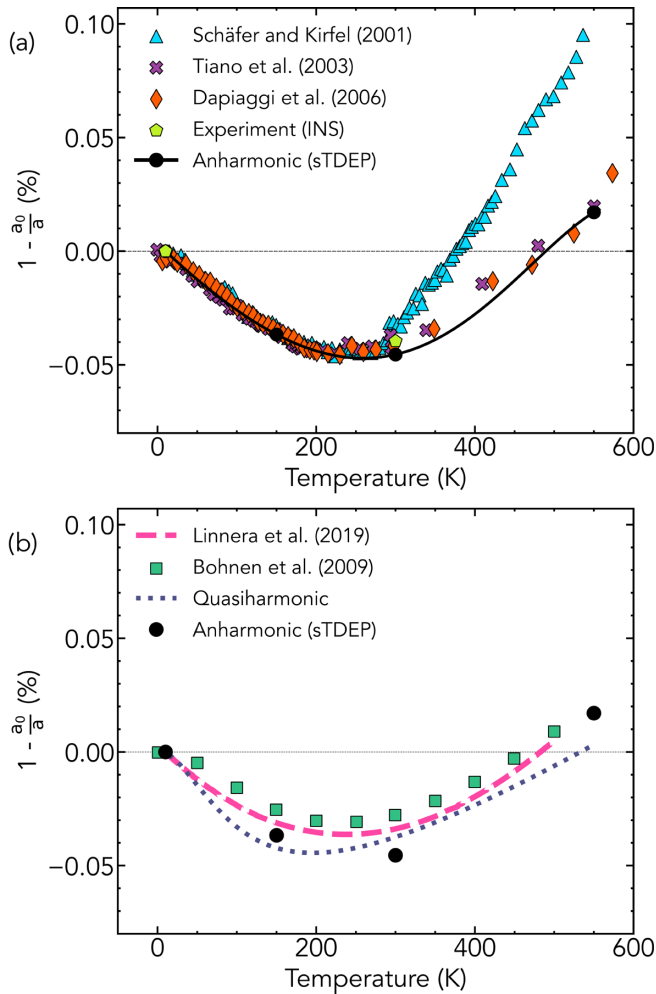


FIG. 7. Percentage change with temperature of lattice parameter of cuprite from experiment and computation. (a) Experimental results [28–30,60] are shown as colored markers compared with anharmonic (AH) result from minimized free energies using sTDEP. (b) Calculated percentage change of lattice parameter vs temperature. Quasi-harmonic (QH) results are colored line and markers [59,61] compared with sTDEP results shown with black circles.

Three-phonon processes are subject to kinematic constraints. The energy constraint requires pairs of lower-energy phonons to add their energy to create a higher-energy phonon. This process alters the self-energies, and Fig. 6 shows peaks at some energies where the self-energy corrections are significant. For example, at 10 K, most of the three-phonon processes involve down-conversion and dominate the high-energy optical modes at 300 K (the self-energy corrections  $>40$  meV are similar at 10 and 300 K). Figure 6 shows that other self-energy corrections become larger at 300 K than at 10 K. Examination of the self-energy corrections and the

phonon partial DOS curves of Fig. 3 shows a large cubic AH of the O-atom optical modes. Modest cubic AH is from acoustic modes dominated by copper atoms.

Below 50 meV, the calculated broadening of phonon dispersions is not as large as the experimental phonon dispersions in Fig. 2. Authors of a previous study attributed some of the thermal behavior of cuprite to quartic AH [64]. Quartic AH contributions can account for further shifts of phonon energies. However, it does not account for phonon lineshapes. This limitation exists because the loop diagram for the quartic term does not have an imaginary part. Higher-order AH processes may be needed to account for the measured thermal broadening and shifts of phonons in cuprite, so it seems challenging for perturbation theory to predict the thermal shifts of phonons in cuprite at higher temperatures.

## VI. CONCLUSIONS

INS with a pulsed neutron source and an area detector with a large solid angle was used to measure all phonons in a single crystal of cuprite at 10 and 300 K. We directly compared phonons from QH calculations, AH calculations, and experiments. AH theory better described the temperature-dependent phonon trends than QH theory. The temperature dependencies of the low-energy TA and high-energy optical modes did not follow the experimental change in volume predicted by QH theory (which was nearly zero in QH theory since the volumes at 10 and 300 K are nearly the same). The calculations with AH theory predicted these shifts better than QH theory. The small NTE in cuprite is calculated successfully with both QH and AH models. However, thermal expansion is an average over numerous phonon contributions to the Gibbs free energy. Thus, thermal expansion may not be the best criterion for revealing the underlying thermodynamics of cuprite. The calculated AH self-energy did not capture the full thermal broadening of the measured optical modes. For cuprite, details of the measured phonon dispersions may require higher-order AH than used here.

## ACKNOWLEDGMENTS

We thank Y. Shen for his insightful comments along with A. Savici for his assistance with data processing. For this paper, we used resources at the Spallation Neutron Source, a U.S. Department of Energy (DOE) Office of Science User Facility operated by the ORNL. For this paper, we used resources from National Energy Research Scientific Computing Center, a DOE Office of Science User Facility supported under Contract No. DE-AC02-05CH11231. This paper was supported by the DOE Office of Science, Basic Energy Sciences, under Award No. DE-FG02-03ER46055.

- [1] W. Mönch, *Semiconductor Surfaces and Interfaces* (Springer, Berlin, Heidelberg, 2001), pp. 1–20.  
 [2] A. Schuster, *London Edinburgh Dublin Philos. Mag. J. Sci.* **48**, 251 (1874).

- [3] Y. Abdu and A. O. Musa, *Rev. Mod. Phys.* **2**, 8 (2009).  
 [4] W. H. Brattain, *Rev. Mod. Phys.* **23**, 203 (1951).  
 [5] K. Mikami, Y. Kido, Y. Akaishi, A. Quitain, and T. Kida, *Sensors* **19**, 211 (2019).

- [6] J. Linnera, G. Sansone, L. Maschio, and A. J. Karttunen, *J. Phys. Chem. C* **122**, 15180 (2018).
- [7] D. Y. Kim, C. W. Kim, J. H. Sohn, K. J. Lee, M. H. Jung, M. G. Kim, and Y. S. Kang, *J. Phys. Chem. C* **119**, 13350 (2015).
- [8] M. B. Gawande, A. Goswami, F.-X. Felpin, T. Asefa, X. Huang, R. Silva, X. Zou, R. Zboril, and R. S. Varma, *Chem. Rev.* **116**, 3722 (2016).
- [9] L. Wan, Q. Zhou, X. Wang, T. E. Wood, L. Wang, P. N. Duchesne, J. Guo, X. Yan, M. Xia, Y. F. Li, A. A. Jelle, U. Ulmer, J. Jia, T. Li, W. Sun, and G. A. Ozin, *Nat. Catal.* **2**, 889 (2019).
- [10] J. Zuo, M. Kim, M. O’Keeffe, and J. Spence, *Nature (London)* **401**, 49 (1999).
- [11] R. J. Elliott, *Phys. Rev.* **124**, 340 (1961).
- [12] K. Huang, *Z. Phys.* **171**, 213 (1963).
- [13] C. Carabatos, *Phys. Stat. Sol.* **37**, 773 (1970).
- [14] J. Hallberg and R. C. Hanso, *Phys. Stat. Sol.* **42**, 305 (1970).
- [15] G. Kugel, C. Carabatos, W. Kress, and H. Id, *J. Phys. Colloques* **42**, C6-884 (1981).
- [16] Y. Petroff, P. Y. Yu, and Y. R. Shen, *Phys. Rev. B* **12**, 2488 (1975).
- [17] A. Compaan, *Solid State Commun.* **16**, 293 (1975).
- [18] P. Dawson, M. M. Hargreave, and G. R. Wilkinson, *J. Phys. Chem. Solids* **34**, 2201 (1973).
- [19] J. Reydellet, M. Balkanski, and D. Trivich, *Phys. Stat. Sol. (b)* **52**, 175 (1972).
- [20] A. Compaan and H. Z. Cummins, *Phys. Rev. B* **6**, 4753 (1972).
- [21] P. Y. Yu, Y. R. Shen, Y. Petroff, and L. M. Falicov, *Phys. Rev. Lett.* **30**, 283 (1973).
- [22] J. C. W. Taylor and F. L. Weichman, *Can. J. Phys.* **49**, 601 (1971).
- [23] M. Balkanski, M. A. Nusimovici, and J. Reydellet, *Solid State Commun.* **7**, 815 (1969).
- [24] E. C. Heltemes, *Phys. Rev.* **141**, 803 (1966).
- [25] M. O’Keeffe, *J. Chem. Phys.* **39**, 1789 (1963).
- [26] K. Reimann and K. Syassen, *Phys. Rev. B* **39**, 11113 (1989).
- [27] G. K. White, *J. Phys. C: Solid State Phys.* **11**, 2171 (1978).
- [28] W. Tiano, M. Dapiaggi, and G. Artioli, *J. Appl. Crystallogr.* **36**, 1461 (2003).
- [29] A. Sanson, F. Rocca, G. Dalba, P. Fornasini, R. Grisenti, M. Dapiaggi, and G. Artioli, *Phys. Rev. B* **73**, 214305 (2006).
- [30] M. Dapiaggi, W. Tiano, G. Artioli, A. Sanson, and P. Fornasini, *Nucl. Instrum. Methods Phys. Res. B* **200**, 231 (2003).
- [31] D. L. Abernathy, M. B. Stone, M. J. Loguillo, M. S. Lucas, O. Delaire, X. Tang, J. Y. Y. Lin, and B. Fultz, *Rev. Sci. Instrum.* **83**, 015114 (2012).
- [32] D. S. Kim, O. Hellman, J. Herriman, H. L. Smith, J. Y. Y. Lin, N. Shulumba, J. L. Niedziela, C. W. Li, D. L. Abernathy, and B. Fultz, *Proc. Natl. Acad. Sci. USA* **115**, 1992 (2018).
- [33] P. B. Allen, *Mod. Phys. Lett. B* **34**, 2050025 (2020).
- [34] T. Mason, D. Abernathy, I. Anderson, J. Ankner, T. Egami, G. Ehlers, A. Ekkebus, G. Granroth, M. Hagen, K. Herwig, J. Hodges, C. Hoffmann, C. Horak, L. Horton, F. Klose, J. Larese, A. Mesecar, D. Myles, J. Neufeind, M. Ohl *et al.*, *Phys. B: Condens. Matter* **385–386**, 955 (2006).
- [35] O. Arnold, J. Bilheux, J. Borreguero, A. Buts, S. Campbell, L. Chapon, M. Doucet, N. Draper, R. Ferraz Leal, M. Gigg, V. Lynch, A. Markvardsen, D. Mikkelsen, R. Mikkelsen, R. Miller, K. Palmén, P. Parker, G. Passos, T. Perring, P. Peterson *et al.*, *Nucl. Instrum. Methods Phys. Res., Sect. A* **764**, 156 (2014).
- [36] J. Y. Y. Lin, F. Islam, and M. Kresh, *JOSS* **3**, 440 (2018).
- [37] S. T. Omelchenko, Y. Tolstova, S. S. Wilson, H. A. Atwater, and N. S. Lewis, in 2015 IEEE 42nd Photovoltaic Specialist Conference (PVSC) (2015), pp. 1–4.
- [38] See Supplemental Material at <http://link.aps.org/supplemental/10.1103/PhysRevB.105.174308> for results from x-ray diffraction measurements and a sample mount photo with the cuprite single crystal. In addition, it includes plots showing intermediary steps in experimental data postprocessing and visualizations of the displaced configurations used for calculations. Detailed explanations accompany these figures and an in-depth description of the theory used in the computations. References [29,39–44] are included.
- [39] L. Y. Isseroff and E. A. Carter, *Phys. Rev. B* **85**, 235142 (2012).
- [40] Y. Shen, C. N. Saunders, C. M. Bernal, D. L. Abernathy, M. E. Manley, and B. Fultz, *Phys. Rev. Lett.* **125**, 085504 (2020).
- [41] M. Kresch, M. Lucas, O. Delaire, J. Y. Y. Lin, and B. Fultz, *Phys. Rev. B* **77**, 024301 (2008).
- [42] A. Werner and H. D. Hochheimer, *Phys. Rev. B* **25**, 5929 (1982).
- [43] V. F. Sears, *Neutron News* **3**, 26 (1992).
- [44] M. D. Lumsden, J. L. Robertson, and M. Yethiraj, *J. Appl. Crystallogr.* **38**, 405 (2005).
- [45] J. L. Niedziela, R. Mills, M. J. Loguillo, H. D. Skorpenske, D. Armitage, H. L. Smith, J. Y. Y. Lin, M. S. Lucas, M. B. Stone, and D. L. Abernathy, *Rev. Sci. Instrum.* **88**, 105116 (2017).
- [46] G. Kresse and J. Hafner, *Phys. Rev. B* **47**, 558 (1993).
- [47] G. Kresse and J. Hafner, *Phys. Rev. B* **49**, 14251 (1994).
- [48] G. Kresse and J. Furthmüller, *Comput. Mater. Sci.* **6**, 15 (1996).
- [49] G. Kresse and J. Furthmüller, *Phys. Rev. B* **54**, 11169 (1996).
- [50] G. Kresse and D. Joubert, *Phys. Rev. B* **59**, 1758 (1999).
- [51] J. Sun, A. Ruzsinszky, and J. P. Perdew, *Phys. Rev. Lett.* **115**, 036402 (2015).
- [52] A. Togo and I. Tanaka, *Scr. Mater.* **108**, 1 (2015).
- [53] O. Hellman, I. A. Abrikosov, and S. I. Simak, *Phys. Rev. B* **84**, 180301(R) (2011).
- [54] O. Hellman, P. Steneteg, I. A. Abrikosov, and S. I. Simak, *Phys. Rev. B* **87**, 104111 (2013).
- [55] O. Hellman and I. A. Abrikosov, *Phys. Rev. B* **88**, 144301 (2013).
- [56] T. H. K. Barron and M. L. Klein, Perturbation theory of anharmonic crystals, in *Dynamical Properties of Solids*, edited by G. Horton and A. Maradudin (North-Holland, Amsterdam, 1974) p. 391.
- [57] A. A. Maradudin and A. E. Fein, *Phys. Rev.* **128**, 2589 (1962).
- [58] D. C. Wallace, *Statistical Physics of Crystals and Liquids* (World Scientific, Singapore, 2003).
- [59] J. Linnera, A. Erba, and A. J. Karttunen, *J. Chem. Phys.* **151**, 184109 (2019).
- [60] W. Schäfer and A. Kirfel, *Appl. Phys. A* **74**, s1010 (2002).

- [61] K.-P. Bohnen, R. Heid, L. Pintschovius, A. Soon, and C. Stampfl, *Phys. Rev. B* **80**, 134304 (2009).
- [62] R. Mittal, S. L. Chaplot, S. K. Mishra, and P. P. Bose, *Phys. Rev. B* **75**, 174303 (2007).
- [63] L. H. N. Rimmer, M. T. Dove, B. Winkler, D. J. Wilson, K. Refson, and A. L. Goodwin, *Phys. Rev. B* **89**, 214115 (2014).
- [64] M. K. Gupta, R. Mittal, S. L. Chaplot, and S. Rols, *J. Appl. Phys.* **115**, 093507 (2014).
- [65] M. M. Beg and S. M. Shapiro, *Phys. Rev. B* **13**, 1728 (1976).
- [66] E. T. Ritz, S. J. Li, and N. A. Benedek, *J. Appl. Phys.* **126**, 171102 (2019).